Supporting Information:

Giant Comprehensive Capacitive Energy Storage in Lead-free Quasi-Linear Relaxor Ferroelectrics via Local Heterogeneous Polarization Configuration

Jikang Liu [a], Chongyang Li[a], Wangfeng Bai[a,b*], Yongjun Yuan[a*],Peng Zheng[a], Qiaolan Fan[a], Shiting Wu[a], Jingji Zhang[c], Jiwei Zhai[d*]

[a]College of Materials and Environmental Engineering, Hangzhou Dianzi University, No. 2 Street, Hangzhou, China

[b]Key Laboratory of Novel Materials for Sensor of Zhejiang Province, Hangzhou Dianzi University, Hangzhou 310012, China

[c]College of Materials Science and Engineering, China Jiliang University, Hangzhou, 310018, China

[d]Functional Materials Research Laboratory, School of Materials Science & Engineering, Tongji University, No. 4800 Caoan Highway, Shanghai, China.

* Corresponding author. E-mail address: bwfcxj@126.com (W.Bai), yjyuan@hdu.edu.cn (Y.Yuan), apzhai@tongji.edu.cn (J.Zhai).

Experimental section

Material preparation: The (1-x) $CaTiO_3$-x $NaNbO_3$ (CT-xNN, x = 0.2, 0.3, 0.4, 0.5) lead-free ceramics were manufactured by the traditional solid reaction method. High-purity oxides and carbonate (≥ 99%) of Na_2CO_3, Nb_2O_5, TiO_2, and $CaCO_3$ powders were selected as the raw materials. The NN powders were calcined at 800 ℃ for 4 h and the CT powders were calcined at 1000 ℃ for 3 h in air. Subsequently, based on the stoichiometric ratio, the resulting powders were weighted and milled for 12 h. Afterward, these powders were mixed with 8 wt% organic binders (PVA) and then pressed into discs. The obtained ceramics disks were sintered at 1150-1350 ℃ for 4-6 h in a sacrificial powder of the same composition and sealed crucibles. To perform ESP measurements, the ceramics were ground and polished to approximately 60-80 μm in thickness and then sputtered with gold electrodes. For dielectric and charging-discharging measurements, the silver paste was coated on two parallel ceramic surfaces, and finally fired at 600 ℃ for 30 min as electrodes.

Characterization：X-ray diffraction with Cu Kα radiation (XRD; MiniFlex600, Rigaku, Japan) and Raman spectroscopy (Horiba/Jobin Yvon, Villeneuve d'Ascq, France) with 532 nm excitation were adopted to analyze the phase structures. The grain morphology and mapping were measured by field-emission scanning electron microscopy (FE-SEM, S-4200, Hitachi, Tokyo, Japan). The piezoelectric force microscopy (PFM, Bruker Dimension Icon) with conductive Platinum-Iridium silicon cantilevers (SCM-PIT, Bruker) was employed to observe the domain structure and analyze the dynamics. Field-emission transmission electron microscope (TEM, FEI Talos F200X, USA) operated at 200 kV was adopted to observe the domain morphology and high-resolution atomic image of the ceramic. For TEM measurements, the ceramics were subjected to ion milling (Gatan 695, USA).

Dielectric properties with respect to temperature and frequency were tested by an LCR meter (Agilent 4990 A, Palo Alto, CA) at a heating rate of 3 ℃/min. The band gap (E_g) of the particle samples was determined by a UV-vis spectrophotometer (TU-1901, Puxi Instruments Technology, China) with an integrating sphere. The

polarization hysteresis (*P-E*) loops with respect to temperature, frequency, cycles and the FORC loops were measured via an FE test system (RT1-Premier II, Radiant Technologies InC, USA). The energy release behavior of ceramic capacitors was evaluated via a commercial charge-discharge platform (CFD-003, Gogo Instruments Technology, China) with a certain discharge resistance, inductance, and capacitance load circuit. The Vickers hardness of the ceramics were obtained under a load of 4.9033 N for 15 s using a Vickers diamond indenter (FALCON 507, INNOVATEST, the Netherlands).

The FORC distribution：In this work, E_{max} is set to be 100 kV/cm, Δα= Δβ= ΔE= 4 kV/cm. An approximate method to calculate $p(\alpha,\beta)$ is

$$p(\alpha,\beta)=\frac{1}{2}\frac{\partial P^2(\alpha,\beta)}{\partial\alpha\partial\beta}\#(1)$$

where $p(\alpha,\beta)$ is the polarization of the FORC loop, α is the reversal electric field, β is the real electric field[1, 2].

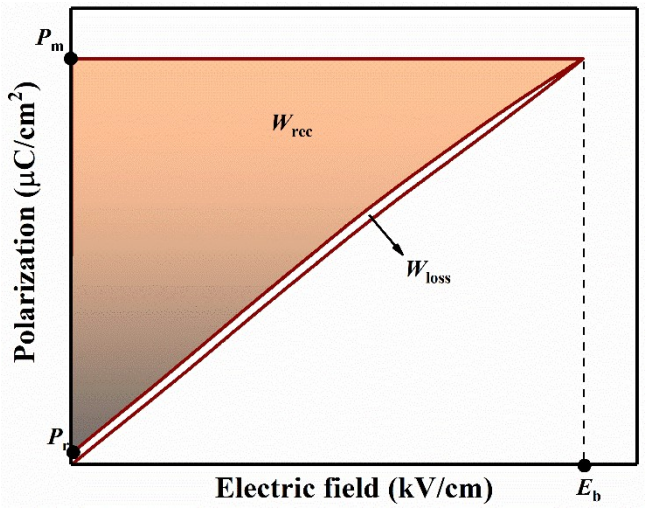

Figure S1. Schematic diagram of *P*-*E* loop for the definition of energy storage performance.

The energy storage performance (W_{rec}, total energy density W, and η) of dielectric capacitors can be calculated by the following formula:

$$W_{rec} = \int_{P_r}^{P_{max}} EdP \#(2)$$

$$W = \int_{0}^{P_{max}} EdP \#(3)$$

$$\eta = \frac{W_{rec}}{W} \times 100\% \#(4)$$

where P_r, P_m, and E denote the remnant polarization, maximum polarization and electric field, respectively [3]. Clearly, in order to realize high W_{rec} and η, large ΔP ($P_{max} - P_r$) and high E_b are required at the same time.

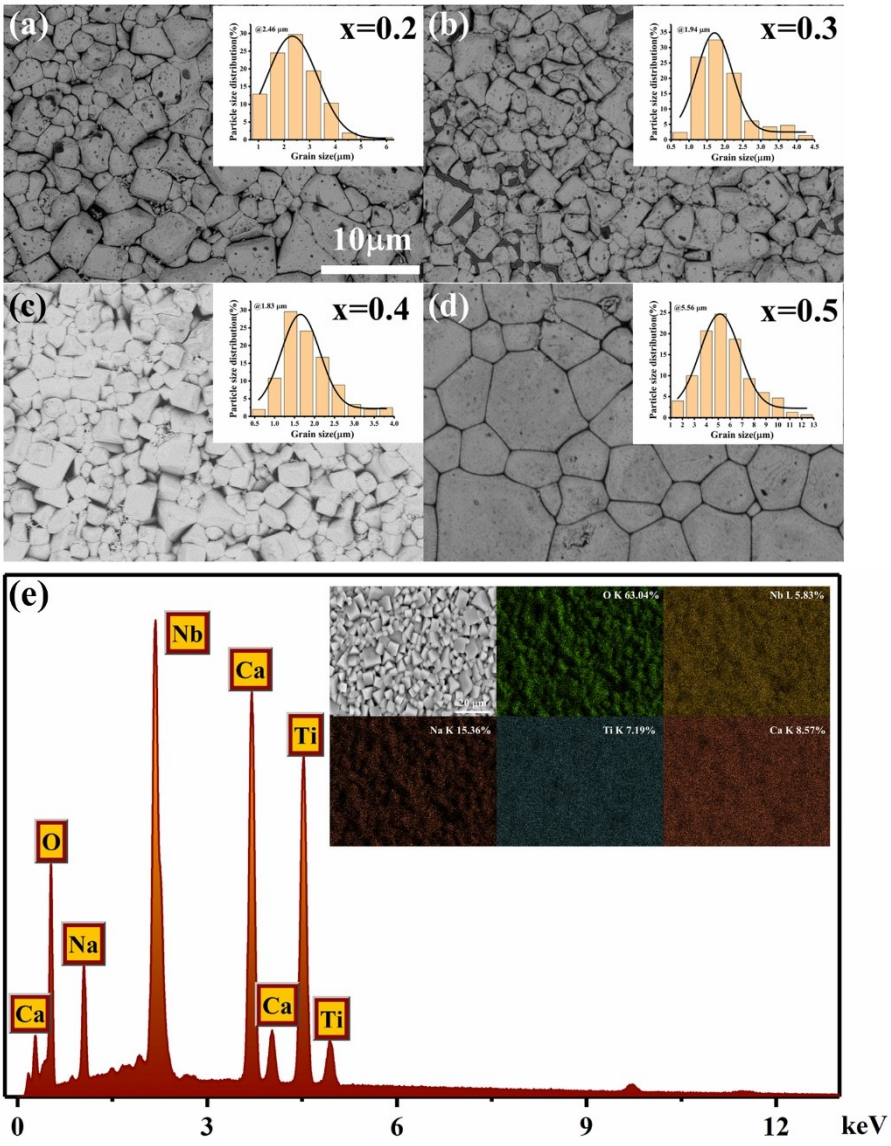

Figure S2. (a-d) SEM images and grain size distributions for CT-xNN ceramics. (e) Energy spectrum and atomic proportion for x=0.4 ceramic.

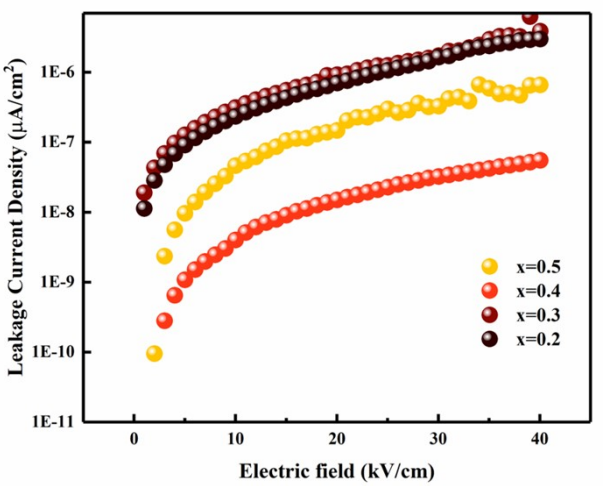

Figure S3. Leakage current density for CT-xNN ceramics.

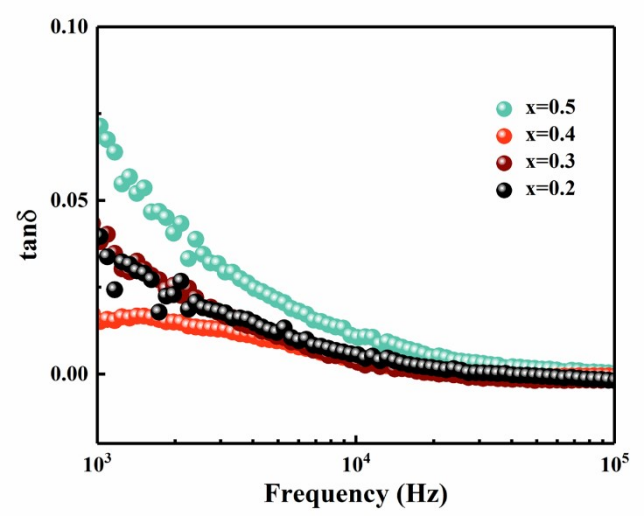

Figure S4. Frequency-dependent dielectric loss for CT-xNN ceramics measured at room temperature.

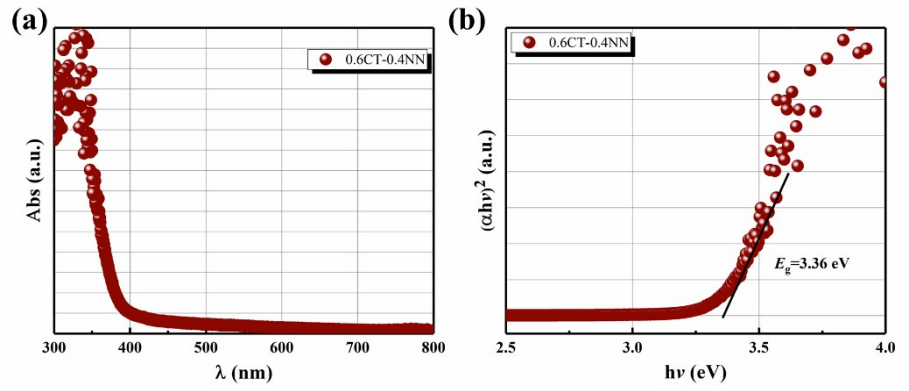

Figure S5. (a) UV-vis absorption spectrum and (b) the dependence of $(\alpha h\nu)^2$ on $h\nu$ for CT-0.4NN ceramic.

The band gap (E_g) can be obtained by the Tauc equation:

$$(\alpha h\nu)^2 = A(h\nu - E_g) \#(5)$$

where $h\nu$, A and α represent photon energy, a constant and absorption coefficient, respectively [4]. The wide E_g will hinder the jump of electrons from the top of the valence band to the bottom of the conduction band, which accounts for a high intrinsic E_b [5, 6].

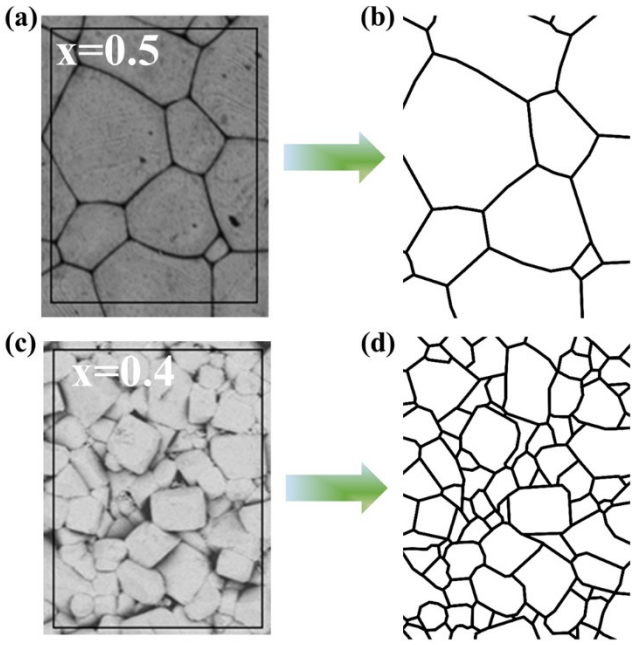

Figure S6. 2D model of x=0.5 (a and b) and 0.4 (c and d) ceramics for finite element simulation calculation.

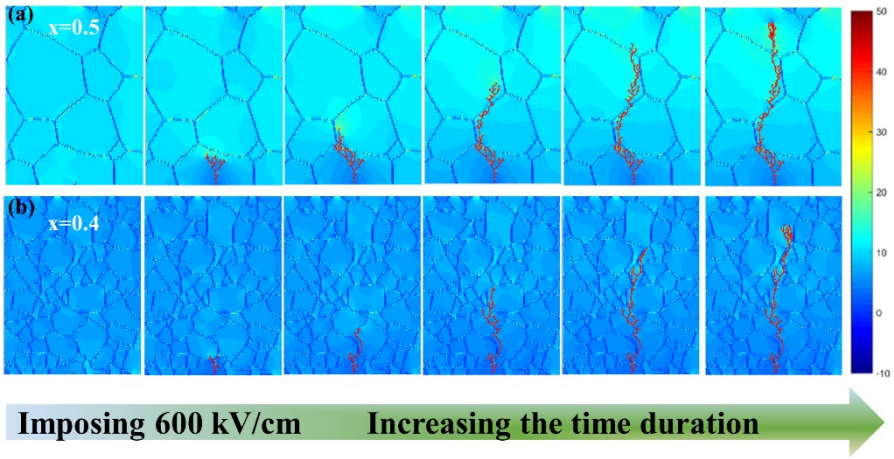

Figure S7. The simulated real-time evolutions of polarization distributions coupled with electrical tree propagation for (a) x=0.5 and (b) x=0.4 ceramics at 600 kV/cm.

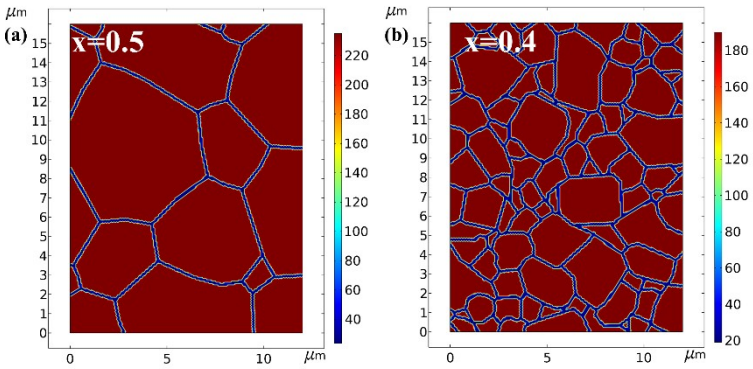

Figure S8. The strong dielectric constant difference between grain and grain boundary for the indicated ceramics.

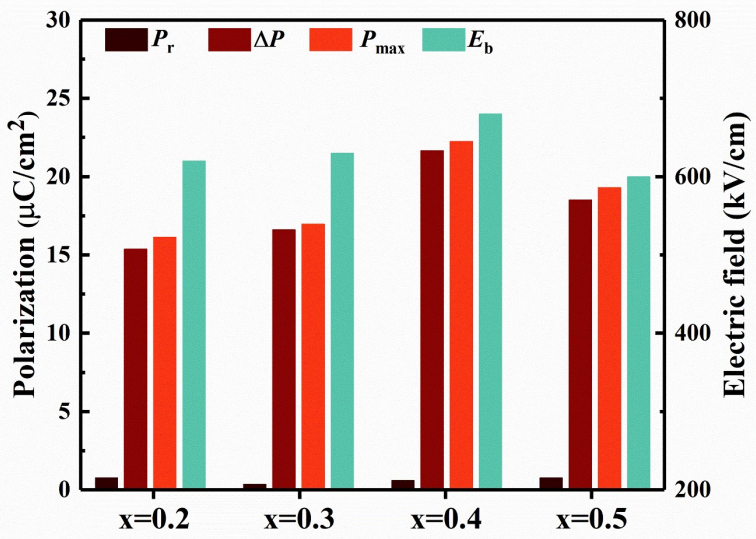

Figure S9. The changes of P_r , ΔP , P_m and E_b for CT-xNN ceramics.

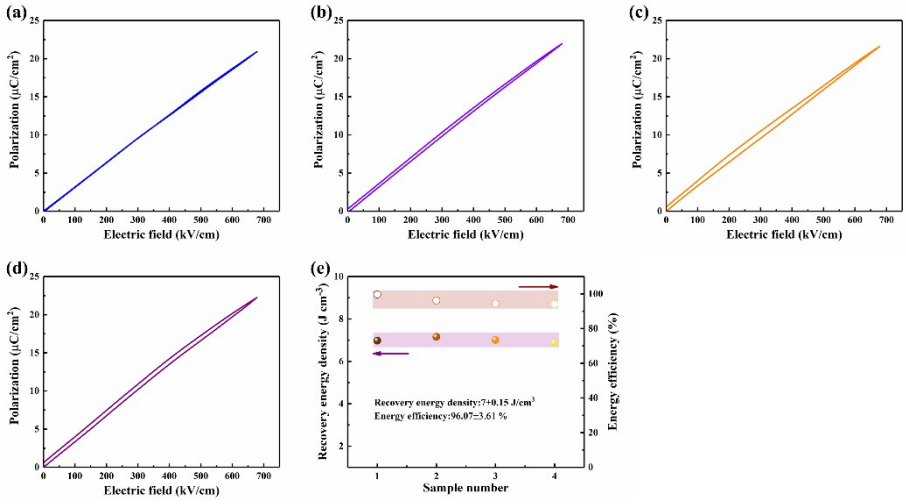

Figure S10. (a)-(d) The *P*-*E* curves of four samples for CT-0.4NN ceramic and (e) the uniformity of W_{rec} and η for CT-0.4NN ceramic.

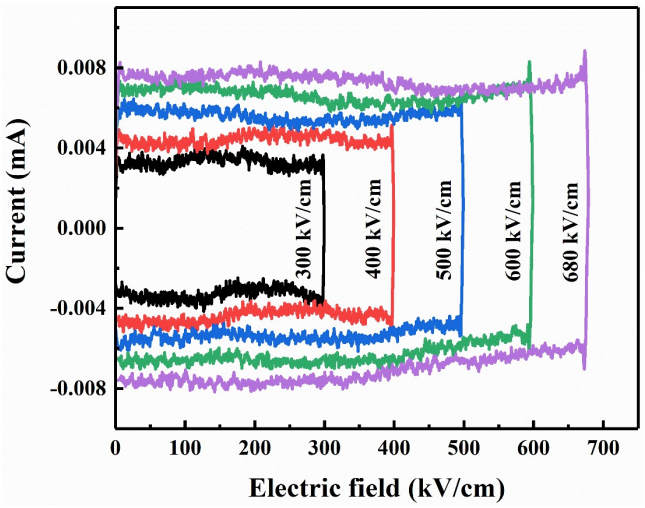

Figure S11. *I-E* curves with respect to the electric field for the CT-0.4NN ceramic.

The *I-E* curves remain flat in shape with no discernible current peak over the whole electric field scope, further indicating the transformation from linear phase to significantly dominated quasi-linear relaxor ferroelectric phase [7], in line with the observation of unipolar *P-E* loops (Fig.3 (a)). This is ascribed to the reinforced reversibility of weakly coupled polar phase induced by the NN addition [6, 8].

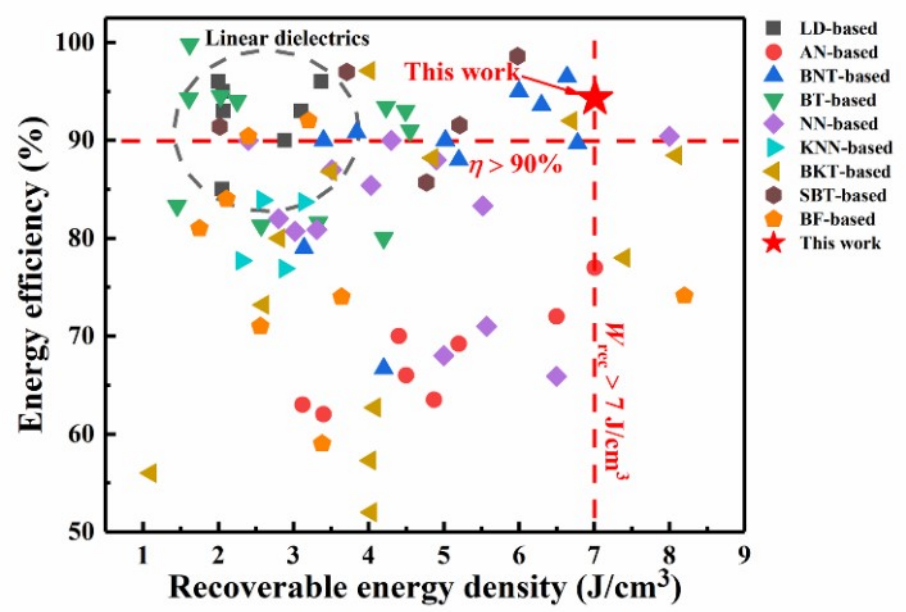

Figure S12. Comparison of the W_{rec} and η of CT-0.4NN ceramic with LD-based, AN-based, BNT-based, BT-based, NN-based, KNN-based, BKT-based, SBT-based and BF-based dielectric ceramics.

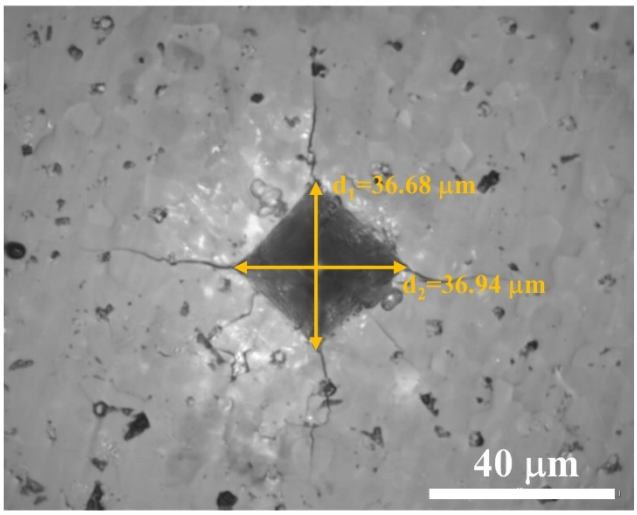

Figure S13. The Vickers diamond indenter's pattern for CT-0.5NN ceramic.

The Vickers hardness H_v can be determined by:

$$H_v = 1.8544\frac{F}{d^2} \#(6)$$

where d is the average value of two diagonal lines (d_1 and d_2), F is the applied force of 4.9033 N [9]. Table S3 provides a summary of the H_v values for CT-0.5NN ceramic.

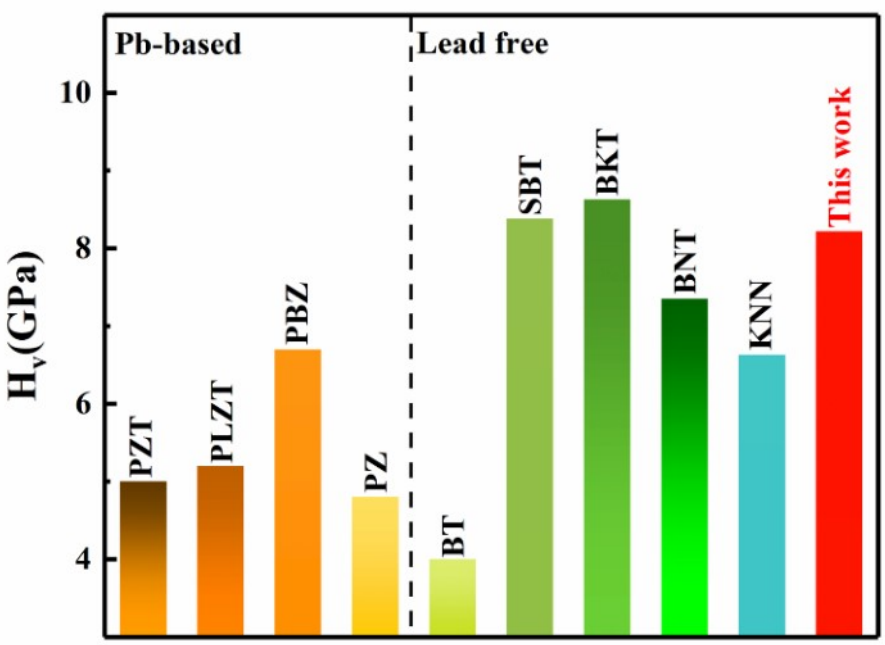

Figure S14. A comparison of H_v and W_{rec} between the CT-0.4NN ceramic and other systems.

In general, fine grain size, compact microstructure, and grain boundary strengthening contribute to the high hardness [10]. In this study, as given in Fig. S2, fine grains (~ 1.83 μm) with compact microstructure accounts for high strength, bringing about a mass of grain boundaries and thus hampering the movement of dislocations [11].

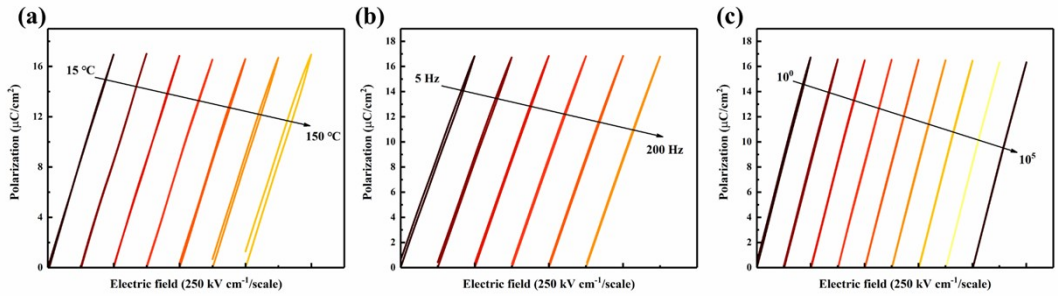

Figure S15. Unipolar *P-E* loops as functions of (a) temperature, (b) frequency and (c) cycling for CT-0.4NN ceramic at fixed electric field of 500 kV/cm.

With increasing the temperature, the W_{rec} and η decrease to a certain degree (Fig. 4(b)). As demonstrated in Fig. 6 (a), the dielectric constant decreases and the dielectric loss increases with the increase of temperature, which lead to the decreased P_m and increased hysteresis. As a consequence, the W_{rec} and η decrease with increasing the temperature.

Indeed, frequency (W_{rec} ~ 4.02 ± 0.06 J/cm^3, 95.8 ± 2.06 %)-insensitive ESP can also be gained. On the one hand, as shown in Fig. 6 (b), stable dielectric constant and a slight decline in dielectric loss can be observed with increasing measuring frequency, which can generate stable P_m and slightly decreased hysteresis with varying frequency, in accordance with the *P-E* loops evolutions with frequency (Fig. S15 (b)). Consequently, the slightly increased W_{rec} and η with the increment of frequency is available, as presented in Fig. 4 (d). On the other hand, the weak correlation between PNRs and high dynamic of them can also ensure ultrafast response of each PNR to applied field, leading to a slim *P-E* loop with a negligible P_r, thus generating satisfactory frequency endurance [8, 12].

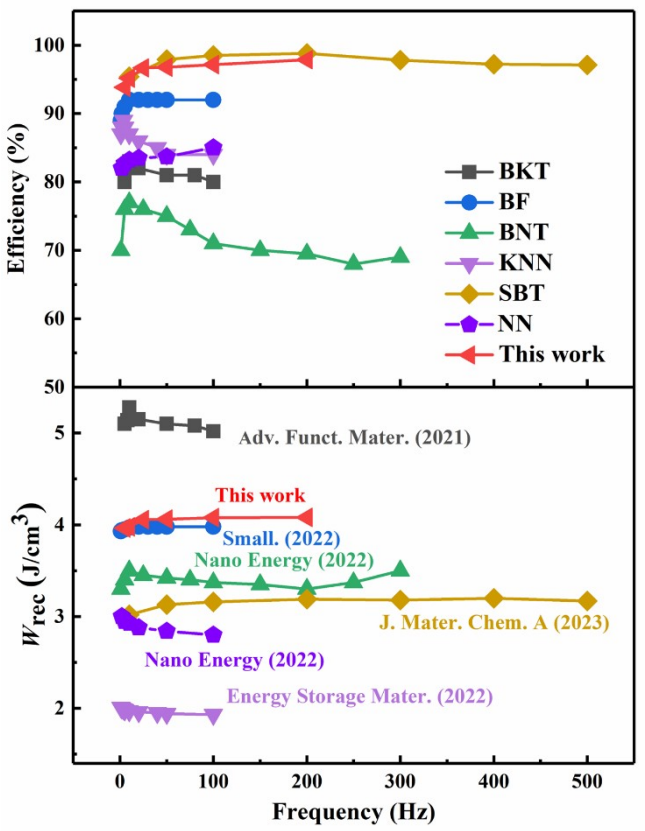

Figure S16. A comparison of W_{rec} and η between the designed ceramic and other recently reported lead-free ceramics with frequency.

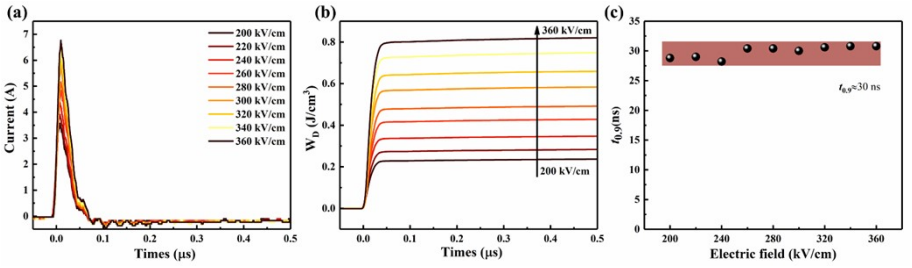

Figure S17. (a) Overdamped discharge waveforms with electric field for CT-0.4NN ceramic. (b) Calculated W_D, and (c) $t_{0.9}$ values under different electric fields for CT-0.4NN ceramic (R = 200 Ω).

The current density (C_D) and power density (P_D) can be calculated from the following formulas [13]:

$$C_D = \frac{I_{max}}{S} \#(7)$$

$$P_D = \frac{EI_{max}}{2S} \#(8)$$

where I_{max}, S, and E are the maximum current, electrode area, and imposed electric field, respectively. The discharged energy density (W_d) can be evaluated from the following relationship [13]:

$$W_D = \frac{R\int I^2(t)dt}{V} \#(9)$$

where R and V denote the load resistor and sample volume, respectively. The W_d of 0.83 J/cm^3 and ultrashort $t_{0.9}$ ≈ 30 ns can be obtained at 360 kV/cm for CT-0.4NN ceramic.

The W_{rec} measured by the *P-E* experiment is higher than W_d measured in the RC circuit at the same electric field, as shown in Fig. 3(e) and Fig. S17 (b). Different mechanisms of the quasistatic *P-E* loop (10^{-1} s) and dynamic discharge measurement with different frequencies (10^{-5} s) are the main contribution for the observed difference between W_d and W_{rec}[14]. In addition, the loss of discharged energy is also linked with the equivalent series resistor, domain walls movement and measurement frequency[15].

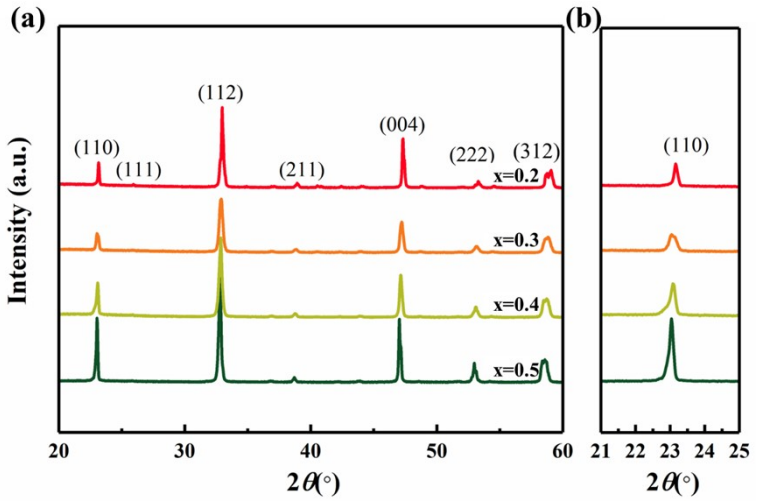

Figure S18. (a) XRD patterns and (b) enlarged 2θ between 21° and 25° of CT-xNN ceramics.

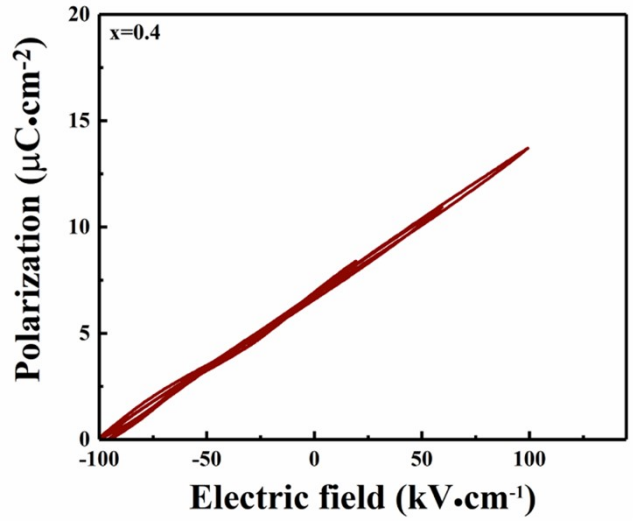

Figure S19. Only 4 out of the 50 total FORC loops for CT-0.4NN ceramic.

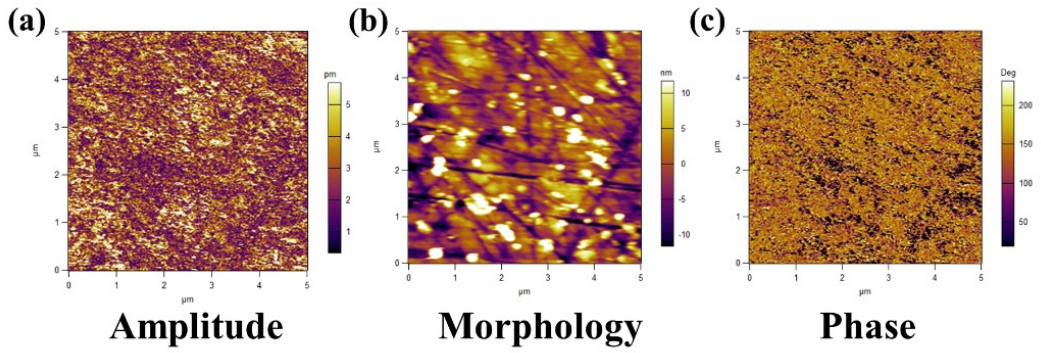

Figure S20. (a)-(c) Out-of-plane PFM amplitude, morphology and phase images for CT-0.4NN ceramic at room temperature.

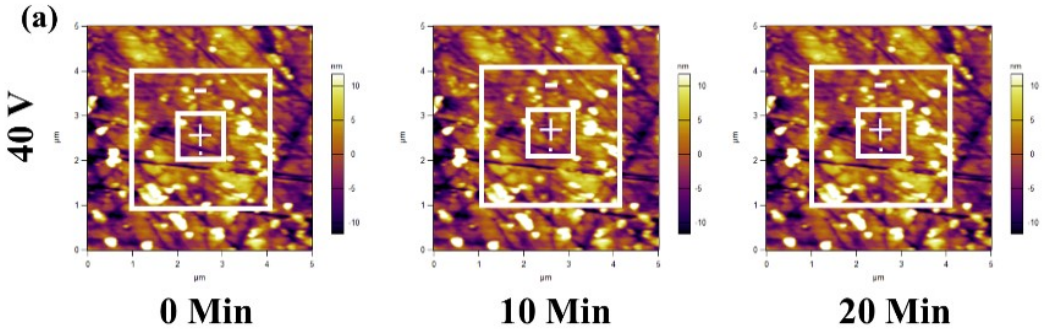

Figure S21. Out-of-plane PFM morphology images for CT-0.4NN ceramic under different relaxor time and 40 V at room temperature.

A negative DC voltage with different amplitude was initially imposed to pole a 3 ×3μm^2 area (larger solid wire frame) and then the same positive voltage was applied to the small internal 1 × 1 μm^2 area (smaller solid wire frame) to explore the reversibility of polarization switching, as shown in Fig. 5 (e) and Fig. S21.

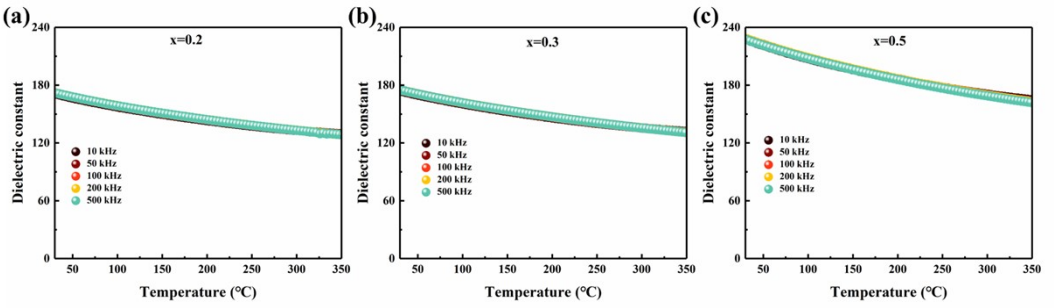

Figure S22. Temperature dependence of dielectric constant from 10 kHz to 500 kHz for (a) x=0.2, (b) x=0.3, and (c) x=0.5 ceramics.

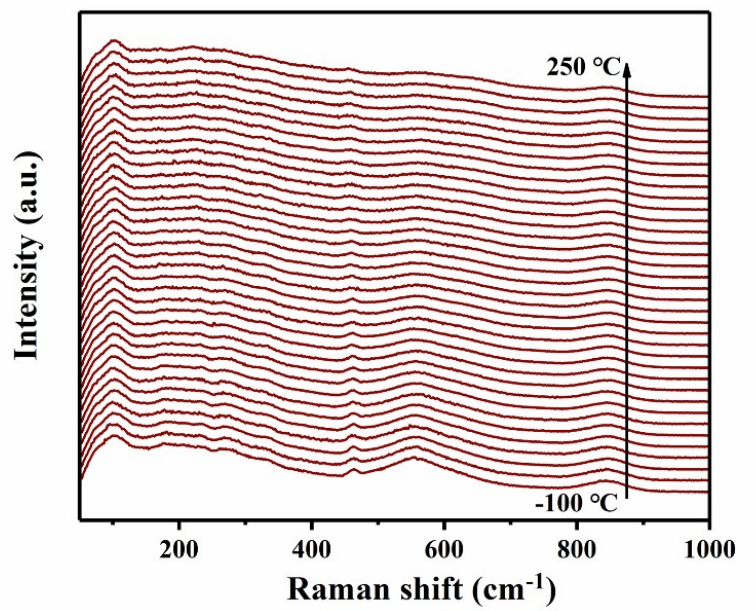

Figure S23. Evolutions of Raman spectra with temperatures for CT-0.4NN ceramic.

Table S1 The comparison of ESP between CT-0.4NN ceramic and previous reports on lead-free energy storage ceramics.

Figure	Ceramics	Ref.
Fig.3(g)	BT-based	16-22
Fig.3(g)	LDs	23-28
Fig.3(g)	SBT-based	29-32
Fig.3(g)	BF-based	12, 33, 34
Fig.3(g)	NN-based	35-37
Fig.3(g)	BNT-based	38-42
Fig.3(g)	KNN-based	43, 44
Fig.3(g)	AN-based	6
Fig.S11	LDs	23-25, 27, 28, 45
Fig.S11	AN-based	46-52
Fig.S11	BNT-based	38, 40-42, 53-56
Fig.S11	BT-based	16, 17, 19-22, 57-59
Fig.S11	NN-based	35, 37, 60-69
Fig.S11	KNN-based	2, 43, 44, 70-77
Fig.S11	BKT-based	11, 78, 79
Fig.S11	SBT-based	29-32
Fig.S11	BF-based	12, 33, 34, 80-84

Table S2 The Vickers hardness values for CT-0.4NN ceramic.

Number	Load/(N)	d_1/(μm)	d_2/(μm)	d_{ave}/(μm)	H_v/(GPa)
1	4.9	33.46	33.18	33.32	8.18
2	4.9	33.73	32.77	33.25	8.22
3	4.9	33.28	32.77	33.03	8.33
4	4.9	33.28	33.45	33.37	8.16
Average					**8.22**

Table S3 The Vickers hardness values for CT-0.5NN ceramic.

Number	Load/(N)	d_1/(μm)	d_2/(μm)	d_{ave}/(μm)	H_v/(GPa)
1	4.9	36.43	37.43	36.93	6.66
2	4.9	36.53	36.31	36.42	6.85
3	4.9	36.68	36.94	36.81	6.71
Average					**6.74**

Table S4 The comparison of the comprehensive performance between CT-0.4NN ceramic and previous reports on lead-free energy storage ceramics.

Figure	Ref.
Fig.4(a)	11, 29, 31, 85, 86
Fig.4(e)	6, 11, 31, 41, 44, 87, 88
Fig.4(h)	6, 11, 44, 88
Fig.S13	11, 29, 85, 86
Fig.S15	2, 11, 29, 89-91

References

1. H. Pan, J. Ma, J. Ma, Q. Zhang, X. Liu, B. Guan, L. Gu, X. Zhang, Y.-J. Zhang, L. Li, Y. Shen, Y.-H. Lin and C.-W. Nan, *Nat. Commun.*, 2018, **9**, 1813.
2. M. Zhang, H. Yang, Y. Lin, Q. Yuan and H. Du, *Energy Stor. Mater.*, 2022, **45**, 861-868.
3. J. Qian, Y. Han, C. Yang, P. Lv, X. Zhang, C. Feng, X. Lin, S. Huang, X. Cheng and Z. Cheng, *Nano Energy*, 2020, **74**, 104862.
4. C. Pascual-Gonzalez, G. Schileo, S. Murakami, A. Khesro, D. Wang, I. M. Reaney and A. Feteira, *Appl. Phys. Lett.*, 2017, **110**, 172902.
5. C. Kim, G. Pilania and R. Ramprasad, *J. Phys. Chem. C*, 2016, **120**, 14575-14580.
6. N. Luo, K. Han, M. J. Cabral, X. Liao, S. Zhang, C. Liao, G. Zhang, X. Chen, Q. Feng, J.-F. Li and Y. Wei, *Nat. Commun.*, 2020, **11**, 4824.
7. B. Yang, Y. Zhang, H. Pan, W. Si, Q. Zhang, Z. Shen, Y. Yu, S. Lan, F. Meng, Y. Liu, H. Huang, J. He, L. Gu, S. Zhang, L.-Q. Chen, J. Zhu, C.-W. Nan and Y.-H. Lin, *Nat. Mater.*, 2022, **21**, 1074-1080.
8. D. Li, D. Zhou, D. Wang, W. Zhao, Y. Guo, Z. Shi, T. Zhou, S.-K. Sun, C. Singh, S. Trukhanov and A. S. B. Sombra, *Small*, 2023, **19**, 2206958.
9. J. Gong, J. Wu and Z. Guan, *J. Eur. Ceram. Soc.*, 1999, **19**, 2625-2631.
10. K. Lu, L. Lu and S. Suresh, *Science*, 2009, **324**, 349-352.
11. L. Chen, F. Long, H. Qi, H. Liu, S. Deng and J. Chen, *Adv. Funct. Mater.*, 2022, **32**, 2110478.
12. H. Qi, A. Xie, A. Tian and R. Zuo, *Adv. Energy Mater.*, 2020, **10**, 1903338.
13. L. Chen, S. Deng, H. Liu, J. Wu, H. Qi and J. Chen, *Nat. Commun.*, 2022, **13**, 3089.
14. J. Li, F. Li, Z. Xu and S. Zhang, *Adv. Mater.*, 2018, **30**, 1802155.
15. J. Li, Z. Shen, X. Chen, S. Yang, W. Zhou, M. Wang, L. Wang, Q. Kou, Y. Liu, Q. Li, Z. Xu, Y. Chang, S. Zhang and F. Li, *Nat. Mater.*, 2020, **19**, 999-1005.
16. X. Dong, X. Li, X. Chen, J. Wu and H. Zhou, *Chem. Eng. J.*, 2021, **409**, 128231.
17. H. Yang, Z. Lu, L. Li, W. Bao, H. Ji, J. Li, A. Feteira, F. Xu, Y. Zhang, H. Sun,

Z. Huang, W. Lou, K. Song, S. Sun, G. Wang, D. Wang and I. M. Reaney, *ACS Appl. Mater. Interfaces*, 2020, **12**, 43942-43949.

18. L. Wu, X. Wang and L. Li, *RSC Adv.*, 2016, **6**, 14273-14282.
19. C. Zhu, Z. Cai, L. Li and X. Wang, *J. Alloys Compd.*, 2020, **816**, 152498.
20. F. Si, B. Tang, Z. Fang, H. Li and S. Zhang, *J. Alloys Compd.*, 2020, **819**, 153004.
21. L. Zhang, L.-X. Pang, W.-B. Li and D. Zhou, *J. Eur. Ceram. Soc.*, 2020, **40**, 3343-3347.
22. Q. Hu, Y. Tian, Q. Zhu, J. Bian, L. Jin, H. Du, D. O. Alikin, V. Y. Shur, Y. Feng, Z. Xu and X. Wei, *Nano Energy*, 2020, **67**, 104264.
23. W. Wang, Y. Pu, X. Guo, T. Ouyang, Y. Shi, M. Yang, J. Li, R. Shi and G. Liu, *Ceram. Int.*, 2019, **45**, 14684-14690.
24. W. Wang, Y. Pu, X. Guo, R. Shi, M. Yang and J. Li, *Ceram. Int.*, 2020, **46**, 11484-11491.
25. T. Ouyang, Y. Pu, J. Ji, S. Zhou and R. Li, *Ceram. Int.*, 2021, **47**, 20447-20455.
26. W. Wang, Y. Pu, X. Guo, R. Shi, M. Yang and J. Li, *J. Alloys Compd.*, 2020, **817**, 152695.
27. W. Wang, Y. Pu, X. Guo, R. Shi, Y. Shi, M. Yang, J. Li, X. Peng and Y. Li, *J. Eur. Ceram. Soc.*, 2019, **39**, 5236-5242.
28. L. Zhang, Y. Pu, M. Chen, T. Wei and X. Peng, *Chem. Eng. J.*, 2020, **383**, 123154.
29. J. Liu, Y. Ding, C. Li, W. Bai, P. Zheng, S. Wu, J. Zhang, Z. Pan and J. Zhai, *J. Mater. Chem. A*, 2023, **11**, 609-620.
30. Y. Ding, P. Li, J. He, W. Que, W. Bai, P. Zheng, J. Zhang and J. Zhai, *Compos. B. Eng.*, 2022, **230**, 109493.
31. C. Zuo, S. Yang, Z. Cao, H. Yu and X. Wei, *Chem. Eng. J.*, 2022, **442**, 136330.
32. P. Zhao, B. Tang, Z. Fang, F. Si, C. Yang, G. Liu and S. Zhang, *J. Materiomics*, 2021, **7**, 195-207.
33. Z. Chen, X. Bu, B. Ruan, J. Du, P. Zheng, L. Li, F. Wen, W. Bai, W. Wu, L. Zheng and Y. Zhang, *J. Eur. Ceram. Soc.*, 2020, **40**, 5450-5457.
34. Q. Li, S. Ji, D. Wang, J. Zhu, L. Li, W. Wang, M. Zeng, Z. Hou, X. Gao, X. Lu,

Q. Li and J.-M. Liu, *J. Eur. Ceram. Soc.*, 2021, **41**, 387-393.

35. D. Lai, Z. Yao, W. You, B. Gao, Q. Guo, P. Lu, A. Ullah, H. Hao, M. Cao and H. Liu, *Ceram. Int.*, 2020, **46**, 13511-13516.
36. L. Yang, X. Kong, Z. Cheng and S. Zhang, *J. Mater. Res.*, 2021, **36**, 1214-1222.
37. H. Chen, J. Shi, X. Chen, C. Sun, F. Pang, X. Dong, H. Zhang and H. Zhou, *J. Mater. Chem. A*, 2021, **9**, 4789-4799.
38. F. Yan, X. He, H. Bai, B. Shen and J. Zhai, *J. Mater. Chem. A*, 2021, **9**, 15827-15835.
39. F. Yan, H. Bai, Y. Shi, G. Ge, X. Zhou, J. Lin, B. Shen and J. Zhai, *Chem. Eng. J.*, 2021, **425**, 130669.
40. D. Li, D. Zhou, W. Liu, P.-J. Wang, Y. Guo, X.-G. Yao and H.-X. Lin, *Chem. Eng. J.*, 2021, **419**, 129601.
41. F. Yan, X. Zhou, X. He, H. Bai, S. Wu, B. Shen and J. Zhai, *Nano Energy*, 2020, **75**, 105012.
42. F. Yang, S. Bao, Y. Zhai, Y. Zhang, Z. Su, J. Liu, J. Zhai and Z. Pan, *Mater. Today Chem.*, 2021, **22**, 100583.
43. Y. Huan, T. Wei, X. Wang, X. Liu, P. Zhao and X. Wang, *Chem. Eng. J.*, 2021, **425**, 129506.
44. D. Li, D. Zhou, D. Wang, W. Zhao, Y. Guo and Z. Shi, *Adv. Funct. Mater.*, 2022, **32**, 2111776.
45. Y. Pu, W. Wang, X. Guo, R. Shi, M. Yang and J. Li, *J. Mater. Chem. C*, 2019, **7**, 14384-14393.
46. J. Gao, Y. Zhang, L. Zhao, K.-Y. Lee, Q. Liu, A. Studer, M. Hinterstein, S. Zhang and J.-F. Li, *J. Mater. Chem. A*, 2019, **7**, 2225-2232.
47. K. Han, N. Luo, S. Mao, F. Zhuo, L. Liu, B. Peng, X. Chen, C. Hu, H. Zhou and Y. Wei, *J. Mater. Chem. A*, 2019, **7**, 26293-26301.
48. N. Luo, K. Han, L. Liu, B. Peng, X. Wang, C. Hu, H. Zhou, Q. Feng, X. Chen and Y. Wei, *J. Am. Ceram. Soc.*, 2019, **102**, 4640-4647.
49. N. Luo, K. Han, F. Zhuo, C. Xu, G. Zhang, L. Liu, X. Chen, C. Hu, H. Zhou and

Y. Wei, *J. Mater. Chem. A*, 2019, **7**, 15450-15450.

50. Y. Xu, Y. Guo, Q. Liu, G. Wang, J. Bai, J. Tian, L. Lin and Y. Tian, *J. Eur. Ceram. Soc.*, 2020, **40**, 56-62.
51. S. Li, T. Hu, H. Nie, Z. Fu, C. Xu, F. Xu, G. Wang and X. Dong, *Energy Stor. Mater.*, 2021, **34**, 417-426.
52. Z. Lu, W. Bao, G. Wang, S.-K. Sun, L. Li, J. Li, H. Yang, H. Ji, A. Feteira, D. Li, F. Xu, A. K. Kleppe, D. Wang, S.-Y. Liu and I. M. Reaney, *Nano Energy*, 2021, **79**, 105423.
53. J. Huang, H. Qi, Y. Gao, A. Xie, Y. Zhang, Y. Li, S. Wang and R. Zuo, *Chem. Eng. J.*, 2020, **398**, 125639.
54. F. Yan, H. Bai, X. Zhou, G. Ge, G. Li, B. Shen and J. Zhai, *J. Mater. Chem. A*, 2020, **8**, 11656-11664.
55. C. Zhu, Z. Cai, B. Luo, L. Guo, L. Li and X. Wang, *J. Mater. Chem. A*, 2020, **8**, 683-692.
56. C. Luo, Q. Feng, N. Luo, C. Yuan, C. Zhou, Y. Wei, T. Fujita, J. Xu and G. Chen, *Chem. Eng. J.*, 2021, **420**, 129861.
57. W.-B. Li, D. Zhou, L.-X. Pang, R. Xu and H.-H. Guo, *J. Mater. Chem. A*, 2017, **5**, 19607-19612.
58. L. Chen, H. Wang, P. Zhao, C. Zhu, Z. Cai, Z. Cen, L. Li and X. Wang, *J. Am. Ceram. Soc.*, 2019, **102**, 4178-4187.
59. D. Meng, Q. Feng, N. Luo, C. Yuan, C. Zhou, Y. Wei, T. Fujita, H. You and G. Chen, *Ceram. Int.*, 2021, **47**, 12450-12458.
60. M. Zhou, R. Liang, Z. Zhou and X. Dong, *J. Mater. Chem. A*, 2018, **6**, 17896-17904.
61. J. Ye, G. Wang, M. Zhou, N. Liu, X. Chen, S. Li, F. Cao and X. Dong, *J. Mater. Chem. C*, 2019, **7**, 5639-5645.
62. J. Chen, H. Qi and R. Zuo, *ACS Appl. Mater. Interfaces*, 2020, **12**, 32871-32879.
63. A. Tian, R. Zuo, H. Qi and M. Shi, *J. Mater. Chem. A*, 2020, **8**, 8352-8359.
64. L. Yang, X. Kong, Z. Cheng and S. Zhang, *ACS Appl. Mater. Interfaces*, 2020,

12, 32834-32841.

65. L. Yang, X. Kong, Z. Cheng and S. Zhang, *J. Mater. Res.*, 2020, **300**, 1-9.
66. X. Dong, X. Li, X. Chen, H. Chen, C. Sun, J. Shi, F. Pang and H. Zhou, *J. Materiomics*, 2021, **7**, 629-639.
67. X. Dong, X. Li, X. Chen, H. Chen, C. Sun, J. Shi, F. Pang and H. Zhou, *Ceram. Int.*, 2021, **47**, 3079-3088.
68. C. Sun, X. Chen, J. Shi, F. Pang, X. Dong, H. y. Chen, K. Wang, X. Zhou and H. Zhou, *J. Eur. Ceram. Soc.*, 2021, **41**, 1891-1903.
69. J. Liu, P. Li, C. Li, W. Bai, S. Wu, P. Zheng, J. Zhang and J. Zhai, *ACS Appl. Mater. Interfaces*, 2022, **14**, 17662-17673.
70. B. Qu, H. Du, Z. Yang, Q. Liu and T. Liu, *RSC Adv.*, 2016, **6**, 34381-34389.
71. B. Qu, H. Du, Z. Yang and Q. Liu, *J. Am. Ceram. Soc.*, 2017, **100**, 1517-1526.
72. T. Shao, H. Du, H. Ma, S. Qu, J. Wang, J. Wang, X. Wei and Z. Xu, *J. Mater. Chem. A*, 2017, **5**, 554-563.
73. X. Ren, L. Jin, Z. Peng, B. Chen, X. Qiao, D. Wu, G. Li, H. Du, Z. Yang and X. Chao, *Chem. Eng. J.*, 2020, **390**, 124566.
74. M. Zhang, H. Yang, D. Li, L. Ma and Y. Lin, *J. Mater. Chem. C*, 2020, **8**, 8777-8785.
75. Y. Zhang and R. Zuo, *J. Eur. Ceram. Soc.*, 2020, **40**, 5466-5474.
76. M. Zhang, H. Yang, Y. Yu and Y. Lin, *Chem. Eng. J.*, 2021, **425**, 131465.
77. A. Manan, A. Ullah, M. A. Khan, A. S. Ahmad, Y. Iqbal, I. Qazi, M. U. Rehman, A. Ullah and H. Liu, *Mater. Res. Bull.*, 2022, **145**, 111521.
78. F. Li, R. Si, T. Li, C. Wang and J. Zhai, *Ceram. Int.*, 2020, **46**, 6995-6998.
79. H. Qi, A. Xie and R. Zuo, *Energy Stor. Mater.*, 2022, **45**, 541-567.
80. N. Liu, R. Liang, X. Zhao, C. Xu, Z. Zhou and X. Dong, *J. Am. Ceram. Soc.*, 2018, **101**, 3259-3265.
81. H. Yang, H. Qi and R. Zuo, *J. Eur. Ceram. Soc.*, 2019, **39**, 2673-2679.
82. H. Sun, X. Wang, Q. Sun, X. Zhang, Z. Ma, M. Guo, B. Sun, X. Zhu, Q. Liu and X. Lou, *J. Eur. Ceram. Soc.*, 2020, **40**, 2929-2935.

83. G. Wang, Z. Lu, H. Yang, H. Ji, A. Mostaed, L. Li, Y. Wei, A. Feteira, S. Sun, D. C. Sinclair, D. Wang and I. M. Reaney, *J. Mater. Chem. A*, 2020, **8**, 11414-11423.
84. N. Liu, R. Liang, Z. Zhou and X. Dong, *J. Mater. Chem. C*, 2018, **6**, 10211-10217.
85. J. Xing, Y. Huang, Q. Xu, B. Wu, Q. Zhang, Z. Tan, Q. Chen, J. Wu and J. Zhu, *ACS Appl. Mater. Interfaces*, 2021, **13**, 28472-28483.
86. X. Li, Y. Cheng, F. Wang, Q. Xu, Y. Chen, L. Xie, Z. Tan, J. Xing and J. Zhu, *Chem. Eng. J.*, 2022, **431**, 133441.
87. Q. Yuan, F.-Z. Yao, S.-D. Cheng, L. Wang, Y. Wang, S.-B. Mi, Q. Wang, X. Wang and H. Wang, *Adv. Funct. Mater.*, 2020, **30**, 2000191.
88. W. Yang, H. Zeng, F. Yan, J. Lin, G. Ge, Y. Cao, W. Du, K. Zhao, G. Li, H. Xie and J. Zhai, *J. Mater. Chem. A*, 2022, **10**, 11613-11624.
89. Z. Che, L. Ma, G. Luo, C. Xu, Z. Cen, Q. Feng, X. Chen, K. Ren and N. Luo, *Nano Energy*, 2022, **100**, 107484.
90. F. Yan, H. Bai, G. Ge, J. Lin, C. Shi, K. Zhu, B. Shen, J. Zhai and S. Zhang, *Small*, 2022, **18**, 2106515.
91. X. Dong, X. Li, X. Chen, Z. Tan, J. Wu, J. Zhu and H. Zhou, *Nano Energy*, 2022, **101**, 107577.